Journal of Alloys and Compounds 827 (2020) 154336

Contents lists available at ScienceDirect

Journal of Alloys and Compounds

journal homepage: http://www.elsevier.com/locate/jalcom

Sandwich layered $Li_{0.32}Al_{0.68}MnO_2(OH)_2$ from spent Li-ion battery to build high-performance supercapacitor: Waste to energy storage approach

Subramanian Natarajan [a], Kaipannan Subramani [b], Yun-Sung Lee [c, **], Marappan Sathish [b, ***], Vanchiappan Aravindan [a, *]

[a] Department of Chemistry, Indian Institute of Science Education and Research (IISER), Tirupati, 517 507, India
[b] Functional Materials Division, CSIR-Central Electrochemical Research Institute (CECRI), Karaikudi, 630 003, Tamil Nadu, India
[c] School of Chemical Engineering, Chonnam National University, Gwang-ju, 61186, Republic of Korea

ARTICLE INFO

Article history:
Received 30 December 2019
Received in revised form
1 February 2020
Accepted 11 February 2020
Available online 12 February 2020

Keywords:
Spent lithium-ion batteries
Asymmetric supercapacitor
Waste to wealth
Bio-waste
Recycling

ABSTRACT

At present, recycling of spent lithium-ion batteries (LIBs) is receiving phenomenal attention owing to valuable resources and make the alternative choice to reutilize the materials in the energy storage applications. Herein, the sandwich layered structure of $Li_{0.32}Al_{0.68}MnO_2(OH)_2$ is successfully regenerated for supercapacitor application *via* reutilizing the different manufacturers of spent LIBs cathodes by considering the upcoming different composition of spent LIBs in the near future. The regenerated layered material by hydrothermal treatment displays a high specific capacitance of 424 F g^{-1} at 1 A g^{-1} and 134 F g^{-1} at a high current density of 10 A g^{-1} in a half-cell configuration. Further, in order to construct high performance and cost-effective asymmetric supercapacitor, the regenerated electrode is paired with bio-waste orange peel derived nanoporous carbon using 3.5 M KOH. The constructed $Li_{0.32}Al_{0.68}MnO_2(OH)_2$/orange peel derived nanoporous carbon ASC exhibits an excellent specific capacitance of 377 F g^{-1}, and delivers a high energy and power density of 42.5 Wh kg^{-1} and 16.5 kW kg^{-1} in the working cell voltage of 1.8 V, respectively. Notably, the constructed ASC holds a long cycle life by retaining 88% capacitance retention after 1,00,000 cycles at 20 A g^{-1}. These outcomes are much higher than those of regenerated material based symmetric supercapacitor. This approach is highly beneficial to recycle the massive quantity of the forthcoming different composition of spent mixed cathodes in the waste stream along with recycled bio-waste to fabricate high-performance energy storage device in the low cost besides to keep the environment in a cleaner and greener manner.

1. Introduction

The increasing domination of fossil fuels from the last few decades in the world's energy consumption strongly affects the environment and the alternative approaches to generating electricity from renewable sources have become a great interest [1–3]. However, the unpredicted climate conditions cause struggle to collect and store the energy from the nonhydroelectric renewable energy sources such as wind and solar, persuaded the researchers to innovate advanced storage technologies [4,5]. Current trending energy storage devices especially lithium-ion batteries (LIBs) could be believed to solve the urgent demand somewhat in the modern electronics and automobile industries owing to the failure of other traditional batteries. The superior features of LIBs including high energy density, hasty charge-discharge rate, protracted cycle life, and environmental friendliness are promising for their practical application [6,7]. Particularly, the development of electric vehicles based on the LIBs has expected to climb from 3 million to 125 million by 2030 as a result of rising CO_2 emissions in the atmosphere [8]. In addition, the LIB market also anticipated to augment from $37.4 billion to $92.2 billion in the time interval of 2018–2024 at a compound annual growth rate (CAGR) of 16.2% [9]. Meanwhile, LIBs ought to meet future demands as the power source for portable electronic devices such as mobile phones,

* Corresponding author.
** Corresponding author.
*** Corresponding author.
E-mail addresses: leeys@chonnam.ac.kr (Y.-S. Lee), msathish@cecri.res.in (M. Sathish), aravind_van@yahoo.com (V. Aravindan).

https://doi.org/10.1016/j.jallcom.2020.154336
0925-8388/

laptops, and digital cameras, etc. This monster growth of LIBs replicates in the demand and price of raw materials such as Li, Co, Mn, Ni and graphite with steep rise [3,10,11].

Exclusively, the lithium demand is likely expected to cross from the current status of 200–500 kt/year in 2025 on a basis of lithium carbonate equivalent which will create the impact on lithium for several years. In Co case, 42% of the production is being directly employed in the fabrication of LIBs, moreover, the required demand would be 222 kt refined equivalent in 2025 which existed only 136 kt in 2017 [12]. The price of other critical metal Ni has expected to reach $50000 per tonne again since the global supply could attain 3 million tonnes by 2030, but with overall demand of 3.8 million tonnes [13]. Therefore, the researches have attempted to produce Co and Ni-free lithium-ion batteries using manganese as the cathode that showed outstanding energy density of ~1000 Wh kg^{-1} in a lab-scale which is quite higher than the existing cathodes energy density of 600–700 Wh kg^{-1} [14]. However, the manganese also unexpectedly surging the demand from LIBs with 23% CAGR from now until 2027, mainly because of the demand for NMC cathodes in the automotive sector [15]. Besides the traditional anode material graphite could lift the requirement to 1747800 tonnes in 2028, and it is calculated only 194160 tonnes in 2017. Currently, some of the researchers are focused to replace the graphite with high-performance anode material for LIBs [16,17]. This scenario raises the questions of how the demand for critical metals going to be met in the future [18].

It is believed that the recycling of damaged/discarded LIBs could help to recuperate the metals and fill the gap of an alternative source for battery materials [3,10]. Apart from this economic value, the undesirable dumping of LIBs in the environment after the lifetime causes severe adverse impacts on human health because of the presence of toxic metals like Co and the liquid electrolyte which contain hazardous organic compounds [19]. Therefore, the recycling of LIBs deserves a huge interest among researchers from the standpoints of environmental safety and natural resource protection. Though it should be revealed that the percentage rate of recycling of LIBs is particularly worrisome as only less than 5% [20]. Moreover, the unprecedented production and sales of electric vehicles along with portable electronics further could produce a different composition of cathode materials (NCM, NCA, LCO, LFP, and LMO, etc.) in a massive amount and alarming the recyclers/industries to develop new recycling methodologies [1,3,10,21]. One of the existing industrial process pyrometallurgies desperately needs high temperature but earns low recovery of metals, while hydrometallurgy process requires low temperature and receives a lot of attention due to the high recovery efficiency [1,21]. In that process, different efforts such as leaching, resynthesis is an emerging technique to recycle the mixed type of cathodes (i.e. different composition including $LiCoO_2$, $LiMn_2O_4$, $LiNi_{1/3}Co_{1/3}Mn_{1/3}O_2$, $LiFePO_4$, etc.) from spent LIBs in a few steps [10,22,23] that could effectively recycle the massive quantity of various manufacturers of spent LIBs in near future. Notably, this type of method avoids the separation of metals from each other after leaching, shortening the metal recovery steps and making it a preferable technique currently to recycle the different composition of spent cathodes [10,21–23].

In this work, we have established the leaching of metals using organic acid from the mixed/different composition of cathodes of various manufacturers, further regenerated the cathode material as a sandwich layered structure of lithium aluminium manganese oxide hydroxide through hydrothermal treatment. Interestingly, the regenerated lithium aluminum manganese oxide hydroxide (LAM) from spent LIBs and nanoporous carbon derived from the orange peel bio-waste (OPAC) has been exploited as a positive and negative electrode, respectively in the fabrication of "asymmetric supercapacitors" for the first time. Usually, layered structure Mn oxide has gained much attention as pseudocapacitive electrode material for supercapacitors owing to the excellent redox properties, high energy density, and good specific capacitance. Additionally, the preparation of activated carbon from bio-waste materials displays an impressive performance in energy storage applications. Therefore, we find a new route here to construct a cost-effective and high-performance ASC by reusing the bio-waste and spent LIBs material as low-cost electrodes that achieved a good specific capacitance of 377 F g^{-1}, long cycle life of 88% of capacitance retention after 100000 cycles at 20 A g^{-1} and high energy density of 42.5 Wh kg^{-1} at 0.5 A g^{-1}.

2. Experimental section

2.1. Renovation of mixed cathodes from spent LIBs

The collected five different manufacturers of mobile phone spent LIBs were discharged in NaCl solution and further dismantled manually to gather metal oxide pasted Al foils (~27%). The remaining parts anode with graphite paste (~18%), plastics (~7.5%), electronic parts (~0.8%) metallic cases (~41%), and the remaining parts were stockpiled to reprocess for more applications. The cathodes from various manufacturers (*i.e.* mixed cathodes) of spent LIBs were reduced into small sizes, subsequently, a low concentration of 1 M HCl and 3.0 v/v % of H_2O_2 were used for the lixiviation at 70 °C for 2 h. Further, valuable metals such as Li, Al, and Mn-containing lixivium was filtered and subjected to the co-precipitation process. The precipitant 3 M LiOH solution was added in dropwise into lixivium at room temperature until the pH of the solution reached 11. Separately, the lixivium was treated with 3 M LiOH up to pH ~11 and transferred into the autoclave for hydrothermal treatment at 90 °C for 72 h. The resultant products were filtered, washed with milli-Q water, and further dried at 70 °C. The obtained material from the mixed cathodes of spent LIBs at room temperature and hydrothermal treatment were finally abbreviated as LAM-RT and LAM-HT, respectively.

2.2. Material characterization

X-ray diffraction (XRD, Bruker D8 Advance, X-ray Diffractometer with Cu Kα radiation, λ = 1.5418 Å) was used to recognize the phase constitution of the regenerated material. Scanning electron microscopy (SEM, JSM-7100F) and transmission electron microscopy (TEM, TECNAI-F20 Philips) were performed to characterize the structure of the renewed materials from the spent LIBs. The surface composition of the regenerated materials was inspected *via* x-ray photoelectron spectra (XPS, Multilab 2000, UK). N_2 adsorption-desorption measurements were performed using an ASAP-2010, Micromeritics sorptometer at 77 K. The composition of the elements present in the obtained materials were measured by ICP-OES (PerkinElmer, Optical 2000 DV). The electrochemical charge storage performance of the regenerated materials was characterized by cyclic voltammetry (CV), galvanostatic charge-discharge (CD) and electrochemical impedance spectroscopy (EIS) technique using BioLogic SP-300, (EC Lab, for three-electrode measurements) and BCS-815 (BT Lab, for full cell measurements) electrochemical workstation. The detailed electrode preparation and fabrication of symmetric and asymmetric supercapacitors are given in supporting information.

3. Results and discussion

3.1. Structure and morphology

Scheme 1 illustrates the recovery and resynthesis of the different composition of spent cathodes from the various

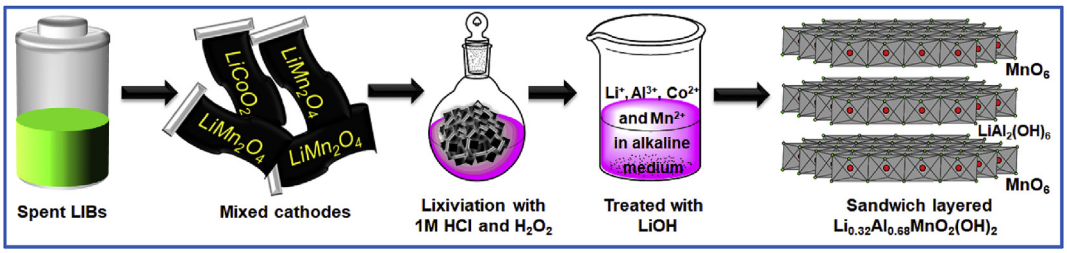

Scheme 1. Regeneration procedure for the sandwich layered of $Li_{0.32}Al_{0.68}MnO_2(OH)_2$ from the different composition of spent LIBs.

manufacturers of spent LIBs. The XRD result (Fig. 1a) specifies that the regenerated material in hydrothermal treatment is composed of stacked cationic $LiAl_2(OH)_6$ octahedral sheets and MnO_6 octahedral anion sheets as like sandwich layered structure in the form of $Li_{0.32}Al_{0.68}MnO_2(OH)_2$ (LAM) [24]. The diffraction peaks of LAM well matched with the standard profile of lithium aluminium manganese oxide hydroxide (ICDD 073–2109) and the material regenerated at room temperature shows broad peaks in amorphous nature as shown in Fig. S1 proves that the room-temperature process efficiently formed the layered structure MnO_2 in the alkaline medium. XPS analysis executed further to confirm the presence of elements and their valence state in the regenerated LAM. As shown in Fig. 1b, the peak 73.4 eV in the Al 2p region indicates the existence of Al (III) [25,26], and the Co 2p spectrum (Fig. 1c) presents two spin-orbit doublets and two satellite peaks after deconvolution. The deconvolution peaks placed at 780.1 (Co $2p_{3/2}$) and 795.2 eV (Co $2p_{1/2}$) are assigned to the Co^{3+} while other binding energy peaks at 782.0 (Co $2p_{3/2}$) and 797.4 eV (Co $2p_{1/2}$) are agreeing to the Co^{2+} [27]. Fig. 1d illustrates the Mn 2p region, authorizes the peaks for Mn^{4+} at 644.3 (Mn $2p_{3/2}$) and 655.6 eV (Mn $2p_{1/2}$) whereas the peaks at 642.1 and 653.8 eV for Mn $2p_{3/2}$ and Mn $2p_{1/2}$ correspond to the Mn^{3+} [27]. The O 1s spectrum of regenerated material is deconvoluted into three peaks at 529.3, 530.7, and 531.9 eV, supportive to the anhydrous Mn–O–Mn, oxygen species along with carbon in the renewed material, and metal hydroxides (Li, Al, Co), respectively [28–30]. Additionally, regenerated LAM-HT was dissolved in the aqua-regia and subjected to ICP-OES analysis to quantify all the possible elements present in the material. In that, the percentage composition of Li, Al, Mn and Co was determined to be 1.0%, 8.4%, 24.5% and 6.3%, respectively which clearly indicates that the manganese dominates majorly in the renewed material.

The morphology of the regenerated material from the spent cathodes was investigated in the FE-SEM analysis that revealed the heterogeneous particle shapes (Fig. 2a and b) and the HR-TEM analysis divulges that the detected lattice fringe with d-spacing of 0.238 nm matching to (−202) plane of the regenerated material (Fig. 2d). The observed selected area electron diffraction (Fig. 2d inset) also further authorizes the crystalline nature of the LAM and the d-spacing 0.46 nm corresponding to the (002) plane which further agrees with the XRD results. Additionally, the N_2 adsorption-desorption measurements of the regenerated material point out the presence of mesopores by displaying typical type IV isotherm (Fig. S2a) and the Brunauer-Emmett-Teller (BET) surface area of LAM-HT touches 107 $m^2\ g^{-1}$ which is less than the BET surface area of LAM-RT 151 $m^2\ g^{-1}$ (Fig. S2b) because of the hydrothermal reaction. Also, the BJH pore size distribution of the LAM-HT demonstrates the pore diameter in the range of 37.7–43.8 nm, however, LAM-RT has a pore diameter around 172 nm indicates the macroporous nature. Moreover, the pore volume of LAM-HT and LAM-RT have calculated to be 0.37 and 0.24 $cm^3\ g^{-1}$. Therefore, the mesoporous nature and high mesopore volume of LAM-HT could ease the diffusion of electrolytes *via* pores to utilize the maximum surface and simultaneously decrease the electron transportation route, which is a great advantage during the charge-discharge process in supercapacitor application.

3.2. Electrochemical analysis

3.2.1. Half-cell configuration of regenerated materials from spent LIBs

In order to examine the electrochemical performance of these regenerated materials as supercapacitor electrodes, electrochemical impedance (EIS), cyclic voltammetry (CV), and galvanostatic charge-discharge (GCD) experiments were performed in the three-electrode configuration using Pt foil and Hg/HgO as counter and reference electrodes, respectively. CVs for both regenerated electrode materials within the voltage range of −0.5 to 0.6 V (*vs.* Hg/HgO) at a scan rate ranging from 5 to 50 mV s^{-1} display more rectangular shapes in a 3.5 M KOH electrolyte solution (Fig. 3a and b). The redox peaks indicate the pseudocapacitance behavior owing to the faradaic redox reactions which permit OH^- distribution from the electrolyte to regenerated electrode surface so as to reach the solution during the redox process. Further, LAM-HT exhibited the specific capacitances of 424, 322, 280, 242, 221 and 134 F g^{-1} and LAM-RT presented 147, 136, 119, 102, 88 and 45 F g^{-1} with GCD measurements at current densities of 1.0, 2.0, 3.0, 4.0, 5.0 and 10.0 A g^{-1} (Fig. 3c and d), respectively. The stability of regenerated materials is evaluated by continuous GCD at a high current density of 10 A g^{-1} for 20,000 long cycles, unveiled an outstanding ~100% capacitance retention for LAM-HT and a gradual decrease ~89% obtained for the mixed hydroxide which was renovated at room temperature (Fig. 3e). This study evidently reveals that both regenerated electrode materials possess good electrochemical stability, however, LAM-HT dominated in the aspects of high capacitance and stability which encourages to assess further in the symmetric and asymmetric cell configurations.

3.2.2. Symmetric supercapacitor using the regenerated LAM-HT material

A symmetric supercapacitor was constructed using the regenerated LAM-HT in an aqueous electrolyte. The CV curves of mixed hydroxide-based symmetric supercapacitor (SSC) exhibit a pseudocapacitive behavior and rate performance from 0 to 1 V at different scan rates of 2–50 mV s^{-1} as shown in Fig. 4a. As the scan rate increased to 50 mV s^{-1}, the CV curve still preserved the rectangular shape, ensuring an admirable rate performance triggered by the mesoporous nature of the regenerated material. The GCD curves of the mixed hydroxide-based SSC at various current densities ranging from 0.2 to 5 A g^{-1} appear nearly symmetric with a linear profile that guarantees the excellent electrochemical reversibility of the regenerated material during the charge-discharge process (Fig. 4b). Notably, the specific capacitance of the SSC device can achieve 392 F g^{-1} at 0.2 A g^{-1} whereas the renovated active material able to deliver the maximum capacitance

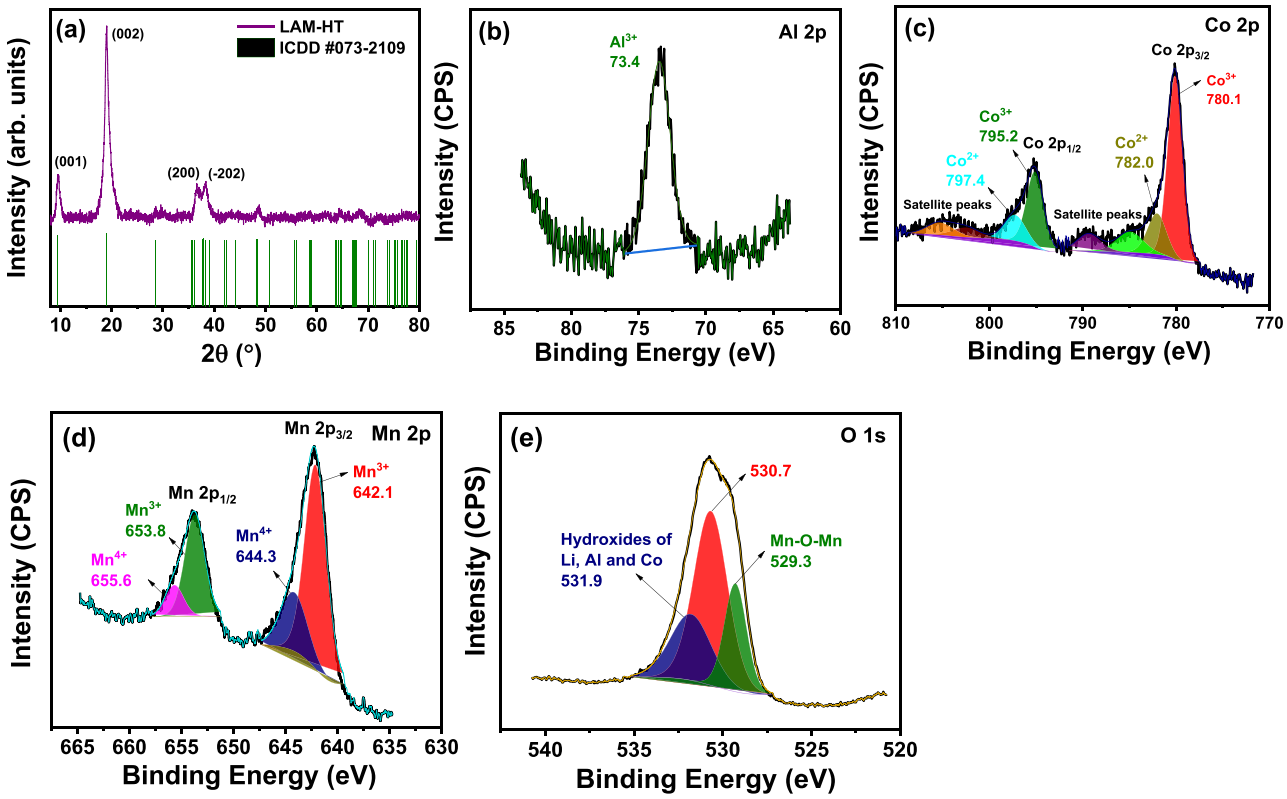

Fig. 1. (a) XRD pattern of sandwich layered LAM-HT; X-ray photoelectron spectra of the (b) Al 2p (c) Co 2p (d) Mn 2p (e) O 1s regions of regenerated LAM-HT.

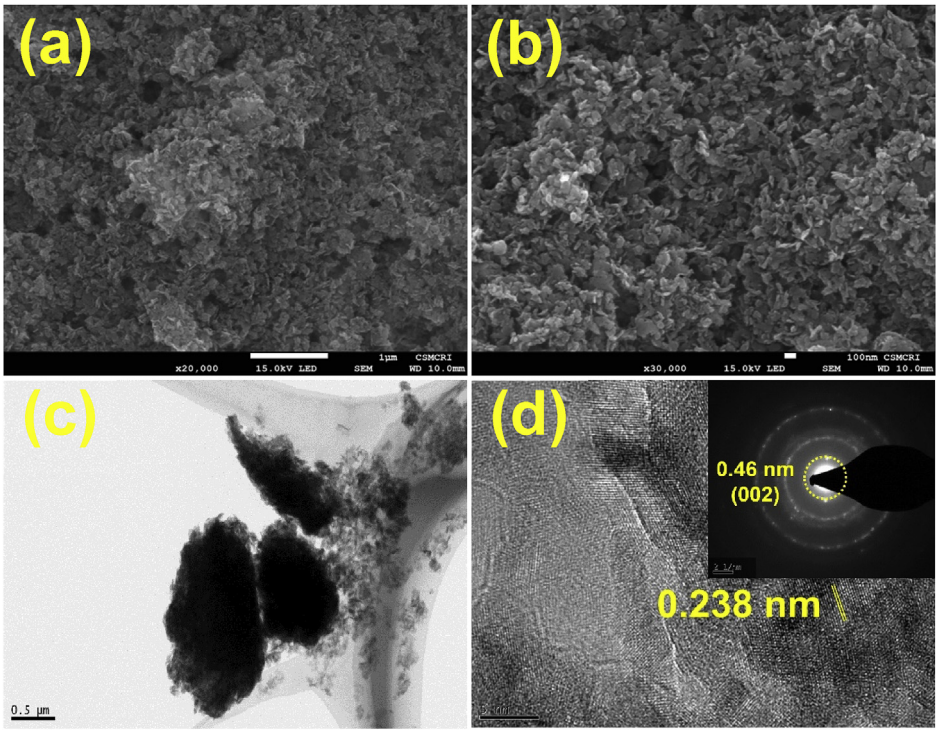

Fig. 2. (a and b) FE-SEM images of regenerated LAM-HT, (c) TEM image and (d) HR-TEM image of regenerated LAM-HT; inset: corresponding SAED pattern.

of 98 F g^{-1}. When the current density increased, the SSC device made up of recycled materials delivered the capacitances of 341, 307, 224 and 52 F g^{-1} at 0.4, 0.8, 1.6 and 5 A g^{-1}, respectively. Moreover, the resultant SSC device comprises of recycled materials offer exceptional cycling stability of 20,000 cycles with ~95% initial capacitance retention at a current density of 5 A g^{-1} (Fig. 4c). The

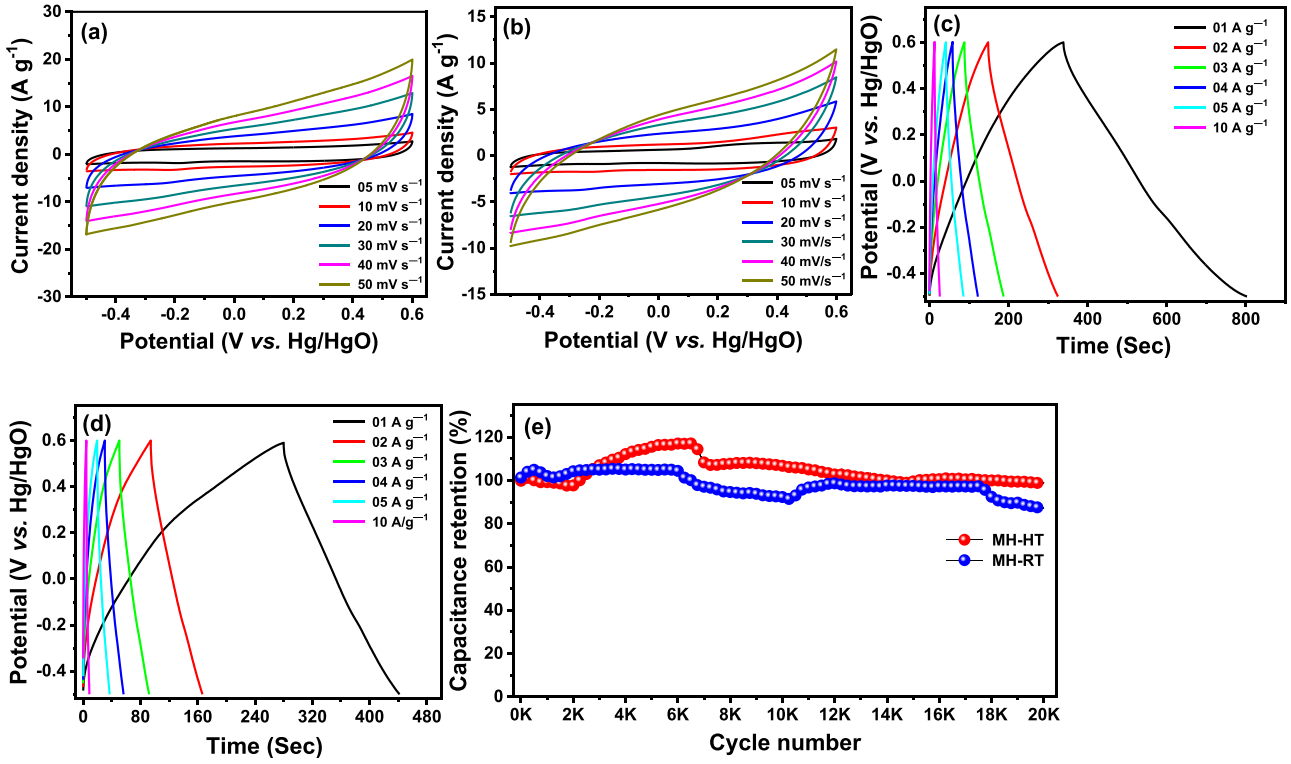

Fig. 3. CV profile of (a) regenerated LAM-HT (b) regenerated LAM-RT electrodes in three-electrode configuration using electrolyte at different scan rates; GCD profile of (c) regenerated LAM-HT (d) regenerated LAM-RT electrodes at different current densities and (e) cycling stability of LAM-HT and LAM-RT electrodes at a high current density of 10 A g^{-1}.

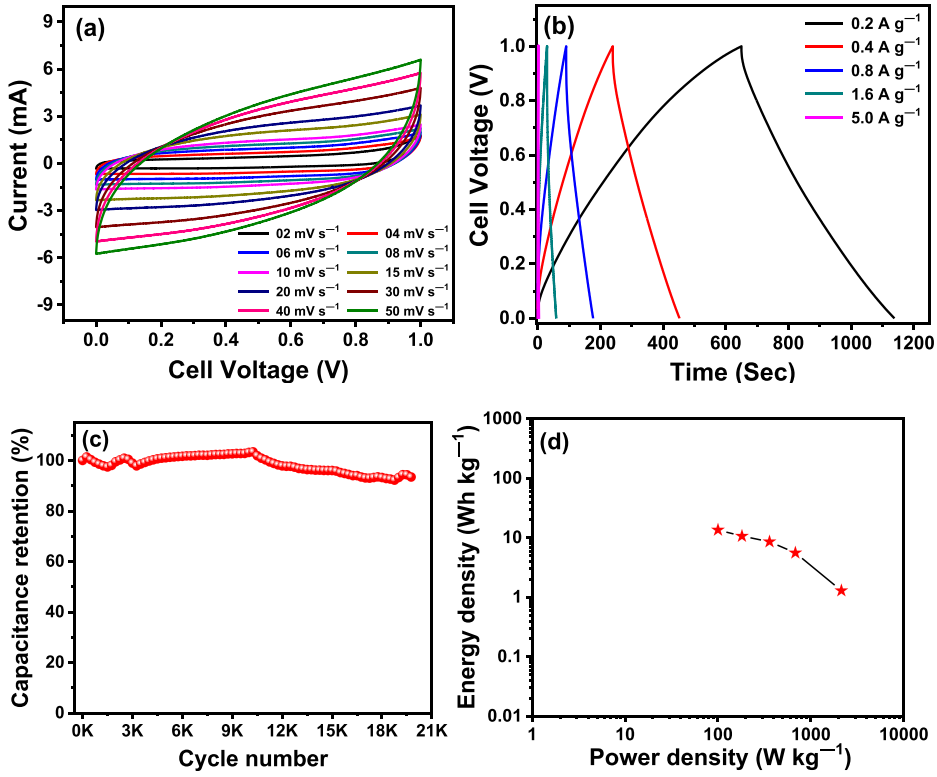

Fig. 4. (a) CV curves of the symmetric device at different working voltages (b) GCD profile of the LAM-HT//LAM-HT symmetric device (c) cyclic stability of the symmetric device (d) Ragone plot for the LAM-HT//LAM-HT symmetric device.

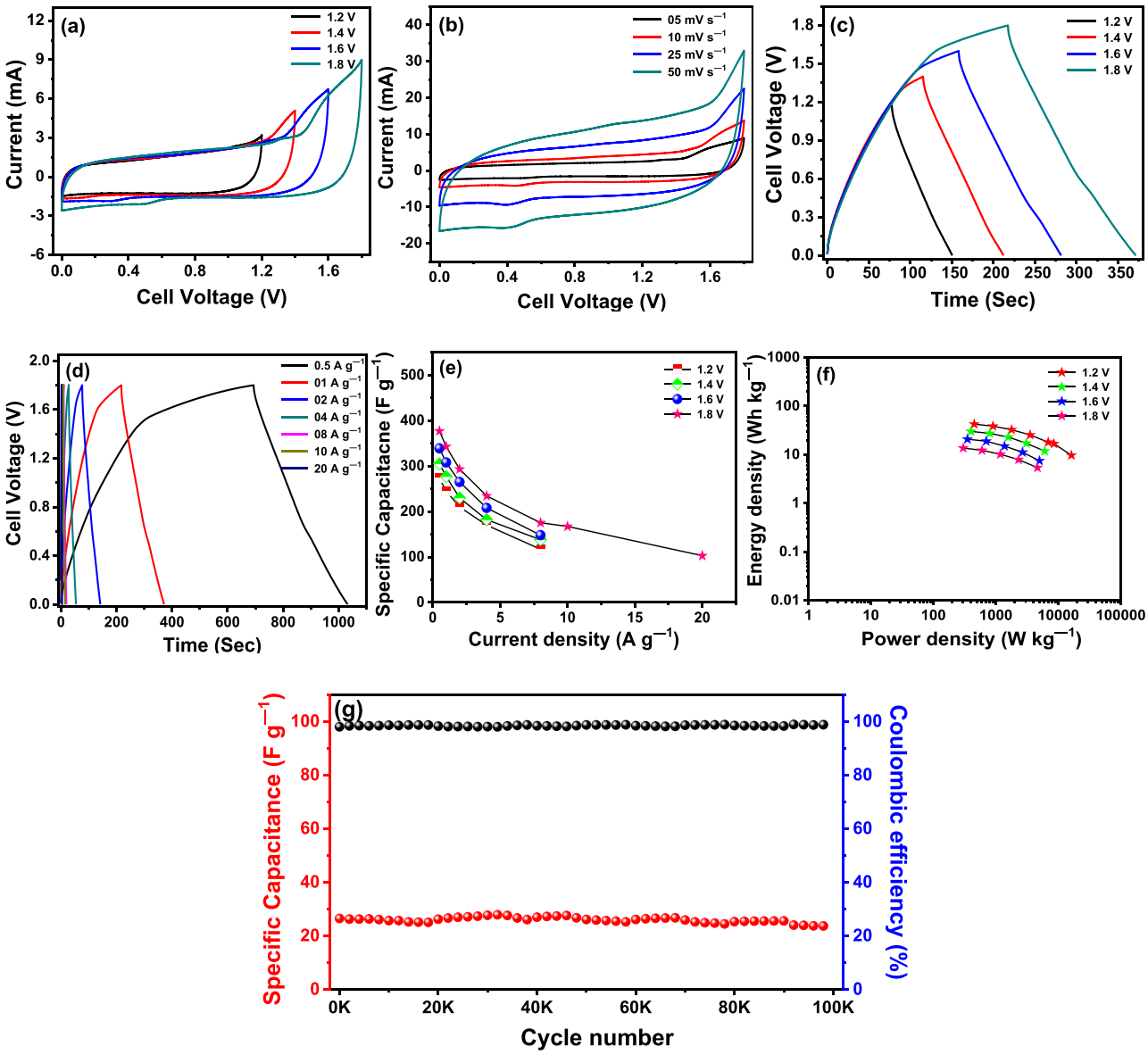

Fig. 5. (a) CV curves of regenerated LAM-HT//OPAC asymmetric supercapacitor device at different working voltages using 3.5 M KOH as electrolyte (b) CV profile of asymmetric device at 1.8 V at different scan rates (c) GCD curves of regenerated LAM-HT//OPAC asymmetric device at different current densities (d) GCD curves of asymmetric device at 1.8 V (e) specific capacitance as a function of current density (f) Ragone plot for the asymmetric device (g) specific capacitance and coulombic efficiency of the asymmetric device as a function of cycle number.

energy and power densities are the decisive factors to assess the practical application of the supercapacitors. Also, we have calculated the energy and power density of the mixed hydroxide-based SSC and plotted the Ragone plot as revealed in Fig. 4d, fetches a maximum energy density of 13.6 Wh kg^{-1} at 100 W kg^{-1} while it brings 1.3 Wh kg^{-1} at a high-power density of 2127 W kg^{-1} induces further to explore in the asymmetric cell configuration. The electrochemical performance of the symmetric device including capacitance, energy and power densities at different current densities is shown in Table S1.

3.2.3. Fabrication of ASC using the recycled materials from spent LIBs and bio-waste

In order to explore the electrochemical performance of regenerated LAM-HT in a two-electrode configuration, it was verified as an ASC using the regenerated LAM-HT and orange-peel derived activated carbon (OPAC) as the positive and negative electrode. The polypropylene spun-bond non-woven fabric was used as a separator for the fabrication of ASC in 3.5 M KOH electrolyte solution and denoted as LAM-HT//OPAC. In this study, the negative electrode material orange-peel derived nano-porous carbon was prepared and characterized as reported previously [31]. The ASC which can be operated at high operating voltage possibly will favour in reducing the number of series for practical applications to attain the output voltage. Typically, the maximum potential asymmetric device could be conquered by combining the different potential of the positive and negative electrodes.

Here, the constructed ASC LAM-HT//OPAC was evaluated at different voltages of 1.2, 1.4, 1.6 and 1.8 V in 10 mV s^{-1} and ensured that the device could stable up to 1.8 V *via* the combination of positive LAM-HT (−0.5 to 0.6 V *vs.* Hg/HgO) and negative OPAC (−0.9 to 0 V *vs.* Hg/HgO) electrodes as shown in the CV profile

Table 1
Comparison of electrochemical performance between the regenerated LAM-HT//OPAC ASC and other MnO_2 based ASC devices.

ASC	Electrolyte	Specific capacitance	Working voltage	Cycles	Energy density	Ref.
Graphene//MnO_2	gel-electrolyte (PVA: H_2SO_4)	–	1.6 V	5000	68 Wh kg^{-1} at 8010 W kg^{-1}	[32]
MnO_2@CNT//CNT	KOH-PVA gel electrolyte	157.53 μF cm^{-1} at 50 mV s^{-1}	1.5 V	10000 with 99% retention	17.26 nWh cm^{-1} at 7.63 μW cm^{-1}	[33]
MnO_2@graphene hydrogel//graphene hydrogel	1 M Na_2SO_4	62.5 at 1 A g^{-1}	2.0 V	2000	34.7 Wh kg^{-1} at 1.0 kW kg^{-1}	[34]
MnO@graphene//AC@MWCNT	0.5 M Na_2SO_4	1.42 F cm^{-2} at a scan rate of 2 mV s^{-1}	1.8 V	1000 cycles with 90%	–	[35]
MnO_2@carbon nanofiber//activated carbon nanofibers	Na_2SO_4	55.7 F g^{-1} at 0.2 A g^{-1}	2.0 V	5000 cycles with 94%	30.6 Wh kg^{-1} at 200 W kg^{-1}	[36]
$NiCo_2O_4$@MnO_2-GF//CNT@GF	1 M Na_2SO_4	2577 F g^{-1} at 1 A g^{-1}	1.5 V	94.3% after 5000 cycles	55.1 Wh kg^{-1} at 187.5 W kg^{-1}	[37]
MnO_2@C//active carbon	5 M $LiNO_3$	307.6 F g^{-1}	2.0 V	96.6% after 1000 cycles	19.9 Wh kg^{-1} at 500 W kg^{-1}	[38]
MnO_2-coated N-doped Activated carbon (N-AC) -multiwalled carbon nanotubes (MWCNT)//N-AC-MWCNT	1 M Na_2SO_4	50.5 F g^{-1} at 2 mA cm^{-2}	1.9 V	88.6% after 5000 cycles	26.4 mWh g^{-1}	[39]
GR@MCNT-MnO_2//GR@MCNT	1 M Na_2SO_4	355 F g^{-1} at 0.3 A g^{-1}	2.0 V	83% after 2500 cycles	28.33 Wh kg^{-1}	[40]
MnO_2/carbon embedded with Ag//Active carbon	3 M KOH	120 F g^{-1} at 1 A g^{-1}	1.7 V	~98.5% after 2000 cycles	48.3 Wh kg^{-1} at 851.7 W kg^{-1}	[41]
graphene@MnO_2//AC	1 M Na_2SO_4	113.5 F g^{-1} at 1 mV s^{-1}	1.8 V	97.3% after 1000 cycles	51.1 Wh kg^{-1} at 102.2 W kg^{-1}	[42]
Recycled mixed cathodes//Orange peel derived activated carbon	3.5 M KOH	377 F g^{-1} at 0.5 A g^{-1}	1.8 V	100000 cycles with 88% retention	42.5 Wh kg^{-1} at 451 W kg^{-1}	This work

(Fig. 5a). Therefore, the stable operating voltage of 1.8 V was preferred in this work to estimate the suitability of regenerated material for the ASC testing. The CV curves of the assembled ASC device at different working voltages of 1.2, 1.4 and 1.6 V are shown in Figs. S3a, S4a, and S5a, respectively. Fig. 5b displays the CV curves of the fabricated LAM-HT//OPAC ASC at various scan rates of 5–50 mV s^{-1} and the curves have not been changed from the rectangular shape when the scan rate increased to 50 mV s^{-1}, specifies the good capacitive behavior of ASC device. Then the GCD analysis at different voltages (Figs. S3b, S4b, and S5b) also supports that the fabricated ASC using renovated material is capable of high-rate applications (Fig. 5c). The charge-discharge curves of LAM-HT//OPAC with a high cell voltage of 1.8 V at various current densities from 1 to 20 A g^{-1} are shown in Fig. 5d. Also, the fabricated ASC device outcomes a maximum specific capacitance of 377 F g^{-1} at a current density of 0.5 A g^{-1} based on the total mass of the two electrodes. However, the capacitance decreased to 343, 293, 234, 175, 167 and 103 F g^{-1} when the scan rate augmented to 1, 2, 4, 8, 10 and 20 A g^{-1}. Fig. 5e shows the comparison of the specific capacitance *vs.* current density of the ASC device at different voltages of 1.2–1.8 V. The Ragone plot (Fig. 5f) for the corresponding energy and power densities for the LAM-HT//OPAC, brings an outstanding energy density of 42.5 Wh kg^{-1} at a power density of 451 W kg^{-1} (0.5 A g^{-1}). Even at a high-power density of 16.5 kW kg^{-1}, the energy density of ASC which is made up of two waste-derived electrodes, retains 9.7 Wh kg^{-1}, comparable to the commercial mixed hydroxide materials. In addition, the cycling stability of the device, the specific capacitance, and coulombic efficiency as a function of the cycle number was measured at a high current density of 20 A g^{-1}. Impressively, the cell maintains 88% capacitance retention even after one lakh cycles with 98.8% coulombic efficiency (Fig. 5g), exemplifying the electrochemical stability of the "waste-derived electrodes". The electrochemical studies result for the ASC device are combined and presented in Table S2. All these electrochemical results guarantee the LAM-HT//OPAC ASC would become a promising energy storage device with the benefits of both high energy and power densities as well as at a low-cost. Additionally, we have compared the electrochemical performance of the LAM-HT//OPAC ASC with other constructed MnO_2//carbon ASC which electrode materials were prepared in a commercial way. As shown in Table 1, the cycling stability of the LAM-HT//OPAC ASC device is much higher than that of ASC in which electrodes are assembled by exploiting the commercial materials and further approving the outstanding performance of the recycled electrode materials from the waste in this work.

4. Conclusion

A novel and efficient recycling route for different manufacturers of spent mixed cathodes (i.e. different composition) by regeneration to high-performance $Li_{0.32}Al_{0.68}MnO_2(OH)_2$ was effectively implemented in this work. In our recycling route, the lixiviation-resynthesis technique has been applied to effectively regenerate the mixed composition of spent cathodes which is a growing technique in the recycling industries to recycle a huge number of various manufacturers of spent LIBs. The regenerated LAM-HT brings an outstanding electrochemical performance when fabricated as a symmetric and asymmetric supercapacitor. The assembled symmetric supercapacitor device reveals a high capacitance of 392 F g^{-1}, possesses a good cycling life of 20,000 cycles by retaining 95% capacitance retention and delivers a maximum energy density of 13.6 Wh kg^{-1} at 100 W kg^{-1}. More importantly, the asymmetric supercapacitor constructed by two waste-derived materials such as regenerated LAM-HT as a cathode and orange-peel derived carbon as anode provides a noteworthy cycling life of 1,00,000 cycles with 88% retention along with 377 F g^{-1} in a high working potential of 1.8 V. Additionally the device presents a high energy density of 42.5 Wh kg^{-1} at 451 W kg^{-1} and could able to deliver 9.7 Wh kg^{-1} at a high power density of 16.5 kW kg^{-1}. This reuse strategy of spent mixed composition of cathodes providing an innovative attentiveness for the recycling of various manufacturers of spent LIBs. Also, this proposed work paves a new idea to develop a high energy density cost-effective energy storage device from the waste-derived materials in the "waste-to-wealth" style.

Declaration of competing interest

The authors declare that they have no known competing financial interests or personal relationships that could have appeared to influence the work reported in this paper.

CRediT authorship contribution statement

Subramanian Natarajan: Conceptualization, Methodology, Writing - original draft, Writing - review & editing, Investigation. **Kaipannan Subramani:** Methodology, Investigation, Visualization, Data curation. **Yun-Sung Lee:** Resources, Validation. **Marappan Sathish:** Resources, Validation. **Vanchiappan Aravindan:** Conceptualization, Supervision.

Acknowledgments

VA acknowledges financial support from the Science & Engineering Research Board (SERB), a statutory body of the Department of Science & Technology, Govt. of India, through the Ramanujan Fellowship (SB/S2/RJN-088/2016). YSL acknowledges the National Research Foundation of Korea (NRF) grant funded by the Korea government (Ministry of Science, ICT & Future Planning) (No. 2019R1A4A2001527). Also, the authors thank the Science & Engineering Research Board, Department of Science and Technology (DST-SERB, File No EMR/2016/006807, GAP 25/17), India for financial support. Further, the authors thank Central Instrumentation Facility, CSIR-CECRI, Karaikudi.

Appendix A. Supplementary data

Supplementary data to this article can be found online at https://doi.org/10.1016/j.jallcom.2020.154336.

References

[1] X. Zhang, L. Li, E. Fan, Q. Xue, Y. Bian, F. Wu, R. Chen, Chem. Soc. Rev. 47 (2018) 7239–7302.
[2] Z. Yang, J. Zhang, M.C.W. Kintner-Meyer, X. Lu, D. Choi, J.P. Lemmon, J. Liu, Chem. Rev. 111 (2011) 3577–3613.
[3] S. Natarajan, V. Aravindan, Adv. Energy Mater. 8 (2018), 1802303.
[4] V. Etacheri, R. Marom, R. Elazari, G. Salitra, D. Aurbach, Energy Environ. Sci. 4 (2011) 3243–3262.
[5] F. Wu, G. Yushin, Energy Environ. Sci. 10 (2017) 435–459.
[6] D. Larcher, J.M. Tarascon, Nat. Chem. 7 (2014) 19.
[7] N. Nitta, F. Wu, J.T. Lee, G. Yushin, Mater. Today 18 (2015) 252–264.
[8] CNBC, Electric vehicles will grow from 3 million to 125 million by 2030, International Energy Agency forecasts, https://www.cnbc.com/2018/05/30/electric-vehicles-will-grow-from-3-million-to-125-million-by-2030-iea.html).
[9] Markets and markets. https://www.marketsandmarkets.com/Market-Reports/lithium-ion-battery-market-49714593.html, 2019, February 15.
[10] S. Natarajan, V. Aravindan, ACS Energy Lett. 3 (2018) 2101–2103.
[11] C. Vaalma, D. Buchholz, M. Weil, S. Passerini, Nat. Rev. Mater. 3 (2018) 18013.
[12] McKinsey & Company, Lithium-and-cobalt-A-tale-of-two-commodities. https://www.mckinsey.com/industries/metals-and-mining/our-insights/lithium-and-cobalt-a-tale-of-two-commodities, 2018, June.
[13] Argus, Nickel prices must rise to meet battery demand: AABC. https://www.argusmedia.com/en/news/1836173-nickel-prices-must-rise-to-meet-battery-demand-aabc.
[14] J. Lee, D.A. Kitchaev, D.-H. Kwon, C.-W. Lee, J.K. Papp, Y.-S. Liu, Z. Lun, R.J. Clément, T. Shi, B.D. McCloskey, J. Guo, M. Balasubramanian, G. Ceder, Nature 556 (2018) 185–190.
[15] W. Boubou, The assay. https://www.theassay.com/technology-metals-edition-insight/manganese-no-longer-just-an-input-on-steel/, 2019, March 7.
[16] Z. Jiang, Y. Li, C. Han, Z. He, W. Ma, W. Meng, Y. Jiang, L. Dai, L. Wang, Ceram. Int. 46 (2020) 1954–1961.
[17] Z. Jiang, Y. Li, C. Han, X. Wu, Z. He, J. Zhu, W. Meng, L. Dai, L. Wang, Ceram. Int. 46 (2020) 4402–4409.
[18] Mining[dot]com, Megafactories buildout could up nickel demand in batteries 19 fold—Benchmark. https://www.mining.com/battery-megafactories-buildout-nickel-demand-19-fold-benchmark/.
[19] S. Natarajan, A.B. Boricha, H.C. Bajaj, Waste Manag. 77 (2018) 455–465.
[20] Editorial, Nat. Energy 4 (2019), 253-253.
[21] W. Lv, Z. Wang, H. Cao, Y. Sun, Y. Zhang, Z. Sun, ACS Sustain. Chem. Eng. 6 (2018) 1504–1521.
[22] Y. Yang, S. Song, F. Jiang, J. Zhou, W. Sun, J. Clean. Prod. 186 (2018) 123–130.
[23] H. Zou, E. Gratz, D. Apelian, Y. Wang, Green Chem. 15 (2013) 1183.
[24] Q. Feng, C. Honbu, K. Yanagisawa, N. Yamasaki, Chem. Mater. 11 (1999) 2444–2450.
[25] J. Zähr, S. Oswald, M. Türpe, H.J. Ullrich, U. Füssel, Vacuum 86 (2012) 1216–1219.
[26] S. Natarajan, H.C. Bajaj, V. Aravindan, J. Mater. Chem. 7 (2019) 3244–3252.
[27] S. Natarajan, S. Anantharaj, R.J. Tayade, H.C. Bajaj, S. Kundu, Dalton Trans. 46 (2017) 14382–14392.
[28] H. Xu, C. Zhang, W. Zhou, G.-R. Li, Nanoscale 7 (2015) 16932–16942.
[29] H.-Q. Wang, J. Chen, S.-J. Hu, X.-H. Zhang, X.-P. Fan, J. Du, Y.-G. Huang, Q.-Y. Li, RSC Adv. 5 (2015) 72495–72499.
[30] K.N. Wood, G. Teeter, ACS Appl. Energy Mater. 1 (2018) 4493–4504.
[31] K. Subramani, N. Sudhan, M. Karnan, M. Sathish, ChemistrySelect 2 (2017) 11384–11392.
[32] H.T. Das, S. Saravanya, P. Elumalai, ChemistrySelect 3 (2018) 13275–13283.
[33] P. Xu, B. Wei, Z. Cao, J. Zheng, K. Gong, F. Li, J. Yu, Q. Li, W. Lu, J.-H. Byun, B.-S. Kim, Y. Yan, T.-W. Chou, ACS Nano 9 (2015) 6088–6096.
[34] X. Meng, L. Lu, C. Sun, ACS Appl. Mater. Interfaces 10 (2018) 16474–16481.
[35] Y. Liu, K. Shi, I. Zhitomirsky, Electrochim. Acta 233 (2017) 142–150.
[36] J.-G. Wang, Y. Yang, Z.-H. Huang, F. Kang, Carbon 61 (2013) 190–199.
[37] M.A. Garakani, S. Abouali, Z.-L. Xu, J. Huang, J.-Q. Huang, J.-K. Kim, J. Mater. Chem. 5 (2017) 3547–3557.
[38] G. Wang, H. Xu, L. Lu, H. Zhao, J. Mater. Chem. 3 (2015) 1127–1132.
[39] K. Shi, I. Zhitomirsky, ChemElectroChem 2 (2015) 396–403.
[40] L. Deng, Z. Hao, J. Wang, G. Zhu, L. Kang, Z.-H. Liu, Z. Yang, Z. Wang, Electrochim. Acta 89 (2013) 191–198.
[41] Y. Guan, Z. Guo, H. Che, J. Mu, X. Zhang, Z. Zhang, G. Wang, Y. Bai, H. Xie, Chem. Eng. J. 331 (2018) 23–30.
[42] Z. Fan, J. Yan, T. Wei, L. Zhi, G. Ning, T. Li, F. Wei, Adv. Funct. Mater. 21 (2011) 2366–2375.